Molecular Therapy
Oncology
Original Article

Intra-tumoral administration of CHST15 siRNA remodels tumor microenvironment and augments tumor-infiltrating T cells in pancreatic cancer

Juanjuan Ye,[1,5] Futoshi Suizu,[1] Keiko Yamakawa,[1] Yuri Mukai,[1] Hiroyuki Yoneyama,[2] Jiro Kondo,[3] Motohiko Kato,[4] Akira Nishiyama,[5] Naohisa Yahagi,[6] and Kyuichi Kadota[1]

[1]Molecular Oncologic Pathology, Department of Pathology and Host-Defense, Faculty of Medicine, Kagawa University, Kita-gun 761-0793, Kagawa, Japan; [2]TME Therapeutics Inc., Minato-ku, Tokyo 105-0021, Japan; [3]Department of Materials and Life Sciences, Sophia University, Chiyoda-ku, Tokyo 102-8554, Japan; [4]Center for Diagnostic and Therapeutic Endoscopy, Keio University School of Medicine, Shinjuku-ku, Tokyo 160-8582, Japan; [5]Department of Pharmacology, Faculty of Medicine, Kagawa University, Kita-gun, Kagawa 761-0793, Japan; [6]Division of Research and Development for Minimally Invasive Treatment, Cancer Center, Keio University School of Medicine, Shinjuku-ku, Tokyo 160-8582, Japan

The dense stroma is one cause of poor efficacy of T cell-mediated immunotherapy in pancreatic ductal adenocarcinoma (PDAC). Carbohydrate sulfotransferase 15 (CHST15) is a proteoglycan-synthetic enzyme responsible for remodeling tumor stroma. Intra-tumoral injection of CHST15 small interfering RNA (siRNA) has been shown to increase the tumor-infiltrating T cells (TILs) in patients with unresectable PDAC. However, the mechanism underlying the enhanced accumulation of TILs is not fully explored. Here, we demonstrate that intra-tumoral injection of CHST15 siRNA locally and remotely diminishes myeloid-derived suppressor cells (MDSCs) and enhances TILs in mice. CHST15 was expressed by tumor cells and MDSCs in both tumor and tumor-draining lymph nodes (TDLNs), and CHST15 siRNA repressed stromal density, neutrophil extracellular traps, and Ly6C/G$^+$ MDSCs *in vivo*. Remarkably, tumor growth inhibition was only observed in the immunocompetent KPC model, which is associated with enhanced TILs. *In vitro*, CHST15 siRNA significantly downregulated the levels of CHST15 and indoleamine 2,3-dioxygenase mRNA in CD33$^+$ MDSCs derived from human peripheral blood mononuclear cells. These results suggest a dual role for intra-tumorally injected CHST15 siRNA on modulating the tumor immune microenvironment for T cell entry and remotely diminishing CHST15$^+$ MDSCs, decreasing T cell suppression and expanding T cells in the TDLN, ultimately leading to an enhanced accumulation of TILs.

INTRODUCTION

Dense stromal remodeling and poor tumor-infiltrating T cells (TILs) are hurdles for the treatment of pancreatic ductal adenocarcinoma (PDAC), especially in patients with unresectable PDAC who did not respond sufficiently or lost response to the first-line chemotherapy. Tumor matrix remodeling has been reported to act as a physical barrier to diminish the efficiency of cancer therapy by interfering with the abilities of systemic drugs and anti-tumor T cells to enter, diffuse, and be activated in the tumor.[1–8] Stroma-modifying agents would thus provide a novel therapeutic strategy to overcome immune suppression and are anticipated to augment effective treatment regimens by combination with chemotherapy and/or immune checkpoint inhibitors.[1–5]

Carbohydrate sulfotransferase 15 (CHST15) is a type II transmembrane Golgi protein that highly biosynthesizes sulfated disaccharide units (E-units) of chondroitin sulfate (CS), which is responsible for tumor matrix remodeling.[9,10] CHST15 and CS-E are involved in the multi-process of tumor progression of a wide range of cancers, including PDAC,[11–24] but their role in immune suppression is largely unexplored. In biopsy specimens from unresectable PDAC patients who showed progression despite first-line gemcitabine and *nab*-paclitaxel therapy, higher CHST15 expression correlated with lower numbers of tumor-infiltrating CD3$^+$ and CD8$^+$ T cells,[25] suggesting the involvement of CHST15 in T cell immune suppression in tumor.

We previously reported that specific knockdown of tumor-intrinsic CHST15 enhanced tumor-infiltrating CD4$^+$ and CD8$^+$ T cells and eliminated tumors in a T cell-dependent manner in a mouse model of PDAC.[26] Comprehensive RNA expression analyses revealed that tumoral CHST15 knockdown up-regulated genes involved in the recognition and killing of cancer cells by T cells, while down-regulated genes related to stromal remodeling and metastasis.[26] The role

Received 13 December 2023; accepted 30 April 2024;
https://doi.org/10.1016/j.omton.2024.200812.

Correspondence: Futoshi Suizu, Oncology Pathology, Department of Pathology and Host-Defense, Faculty of Medicine, Kagawa University, Kita-gun, Kagawa 761-0793, Japan.
E-mail: suizu.futoshi@kagawa-u.ac.jp
Correspondence: Kyuichi Kadota, Oncology Pathology, Department of Pathology and Host-Defense, Faculty of Medicine, Kagawa University, Kita-gun, Kagawa 761-0793, Japan.
E-mail: kadota.kyuichi@kagawa-u.ac.jp

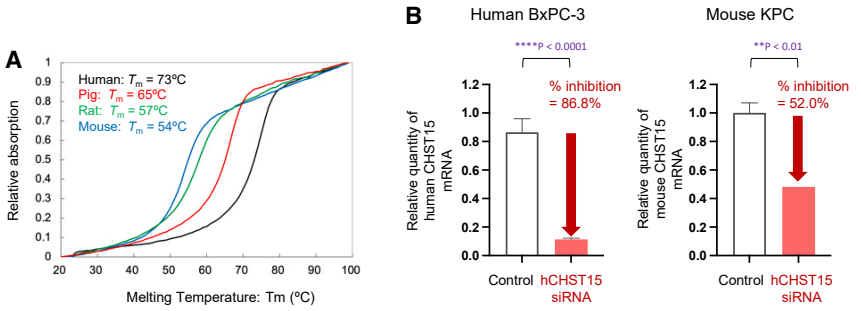

Figure 1. Comparison of hCHS15 siRNA's binding affinity to and silencing efficacy on human and mouse mRNAs

(A) Binding affinity of hCHST15 siRNA to human (black), pig (red), rat (green), and mouse (blue) CHST15 mRNAs. Melting temperatures are shown. (B) *In vitro* silencing efficacy of hCHST15 siRNA on human CHST15 mRNA by human BxPC-3 cells and mouse CHST15 mRNA by mouse KPC cells are shown. Relative quantity was measured compared with control by qPCR. ****p < 0.0001, **p < 0.01, Welch's independent t test.

of tumor-intrinsic CHST15 in the suppression of anti-tumor activity by T cells was shown in mice.[26]

In a phase 1/2a clinical study, intra-tumoral administration of STNM01, the RNA oligonucleotide to suppress CHST15 gene expression through an RNA interference mechanism,[25,27–34] significantly increased tumor-infiltrating $CD3^+$ and $CD8^+$ T cells in patients with chemotherapy-refractory, unresectable PDAC as a second-line therapy.[25] An increase in $CD3^+$ T cells at week 4 after the first dose of STNM01 correlated with longer survival, indicating that treatment-associated rapid increase of TILs contributed to favorable outcomes.[25] One possibility is that STNM01 acted locally and broke the physiological matrix barrier, leading to accelerated recruitment of anti-tumor T cells into the tumor. However, questions arose if anti-tumor T cells were sufficiently induced or expanded before entering into the tumor site, as T cells were poorly detectable in immunosuppressive PDAC patients of second-line setting. Thus, in the present study, we investigated how locally injected human CHST15 small interfering RNA (siRNA), which has the same sequence as STNM01, enhances TILs in *vivo* in mouse models of PDAC.

RESULTS

Comparison of human CHST15 siRNA's binding affinity to and silencing efficacy on human and mouse mRNAs

To investigate the *in vivo* mechanism underlying the increased TILs by intra-tumoral STNM01 application found in clinical studies in patients with unresectable PDAC, the present study was conducted under several conditions in mice. First, we used human CHST15 siRNA (hCHST15 siRNA), which has the same sequence as STNM01, but not mouse CHST15 siRNA. Second, both T cell-deficient nude mice and immunocompetent mice were used as a hosts, to examine the differences in tumor lesions in the presence or absence of T cells. Third, we selected PDAC cell lines whose proliferation was not affected by CHST15 silencing *in vitro*, to examine immune-mediated tumor growth inhibition by excluding the influence of *in vivo* anti-proliferative effects as much as possible. Therefore, human BxPC-3 cells and mouse KPC cells were selected, as the proliferation of these cells was not affected by several CHST15 silencing methods *in vitro* in our preliminary and past studies (Figure S2).[26]

Melting temperature analysis showed that antisense oligonucleotides of hCHST15 siRNA designed to be fully complementary to the *Homo sapiens* (human) RNA sequence hybridized most strongly with it. In addition, the antisense oligonucleotide hybridized with the corresponding RNA sequences of *Sus scrofa domesticus* (pig), *Rattus norvegicus* (rat), and *Mus musculus* (mouse), even though these hybridized complexes include several base mismatches (Figure 1A; Table S2). The melting temperature tended to decrease as the number of base mismatches increased. The decreased binding affinity of hCHST15 siRNA to mouse CHST15 mRNA was consistent with decreased silencing efficacy *in vitro* that hCHST15 siRNA showed 86.8% knockdown against human CHST15 mRNA in BxPC-3 cells and 52.0% against mouse CHST15 mRNA in KPC cells (Figure 1B). However, the inhibition rate of mouse CHST15 mRNA by hCHST15 siRNA was significant compared with that by control.

hCHST15 siRNA showed tumor growth inhibition in immunocompetent mice

In human BxPC-3-implantation model in T cell-deficient nude mice, hCHST15 siRNA or control vehicle was injected intra-tumorally twice a week from day 28, and mice were sacrificed at day 42 (Figure 2A). In a murine KPC-implantation model in immunocompetent mice, hCHST15 siRNA or control vehicle was injected intra-tumorally twice a week from day 7 and mice were sacrificed at day 21 (Figure 2B).

In T cell-deficient mice, there was no significant difference in tumor size (Figure 2C); in contrast, tumor growth was inhibited in the immunocompetent mice (Figures 2C and 2D).

Intra-tumoral injection of hCHST15 siRNA altered tumor stromal components in both human BxPC-3 and murine KPC tumor models

We first investigated the stromal components by histological examination. CHST15 protein was positive for ductal tumor cells in control mice (Figure 3A) and hCHST15 siRNA significantly repressed CHST15 positive area (Figure 3A). The dense deposit of collagen fibers and fibrils was seen and this was associated with massive citrullinated histone H3 staining, a hallmark of neutrophil extracellular trap (NET) formation, and poor $CD31^+$ vascularity (Figure 3A).

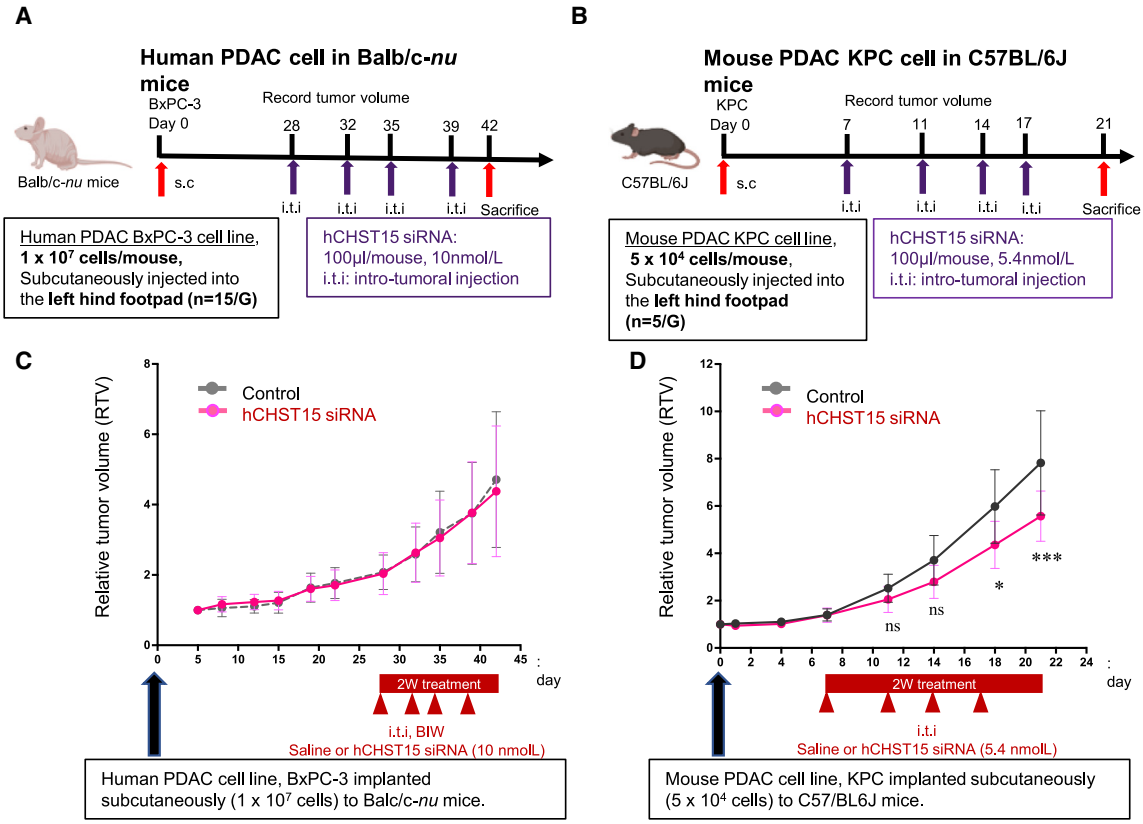

Figure 2. hCHST15 siRNA showed tumor growth inhibition in immunocompetent mice

(A and C) Human BxPC-3 cells (1×10^7 cell/mouse) were implanted subcutaneously into Balb/c-nu mice on day 0, and macroscopic tumor volume was monitored (n = 15). ns, not significant by two-way ANOVA with Bonferroni multiple comparison test. (B and D) Mouse KPC cells (5×10^4 cell/mouse) were implanted subcutaneously into syngeneic C57/BL6 mice on day 0, and macroscopic tumor volume was monitored (n = 5). *p < 0.05, ***p < 0.001. ns, not significant by two-way ANOVA with Bonferroni multiple comparison test.

In contrast, collagen formation was sparse in hCHST15 siRNA-treated mice (Figure 3A). hCHST15 siRNA markedly decreased the citrullinated histone $H3^+$ NET formation while increasing the $CD31^+$ vascularity (Figure 3A). Accumulation of $Ly6C/G^+$ myeloid-derived suppressor cells (MDSCs) within the fibrotic area was also detected in control, and this was reduced by hCHST15 siRNA (Figure 3A).

CHST15 was strongly expressed by tumor cells (Figure 3B) and stromal remodeling, such as dense fibrotic architecture, NETosis, and aberrant vascularity was seen in control mice (Figure 3B). Massive accumulation of MDSCs was seen (Figure 3B) and greater positivity of CHST15 and MDSC was observed in immunocompetent control mice compared with T cell-deficient control mice (Figures 3A, bottom, and 3B, bottom). hCHST15 siRNA significantly reduced percent positive areas of CHST15 and this was associated with reduced fibrotic structure, NETosis, and MDSCs (Figure 3B). Part of the accumulated MDSCs expressed CHST15, and hCHST15 siRNA repressed these cells (Figure S3). These results indicated that suppressed stromal remodeling by hCHST15 siRNA was a common feature in both immunodeficient and immunocompetent mice.

hCHST15 siRNA showed enhancement of T cells in both the tumor and TDLN in the KPC model

In the KPC model, tumor-infiltrating $CD4^+$ and $CD8^+$ T cells were rarely detectable in control mice (Figure 4A). In contrast, we found a significant increase in the number of tumor-infiltrating $CD4^+$ and $CD8^+$ T cells by intra-tumoral injection of hCHST15 siRNA (Figure 4A). In addition, Ki-67^+ proliferating $CD4^+$ and $CD8^+$ T cells were rarely detectable in control mice as well, while significantly increased by locally injected hCHST15 siRNA (Figure 4B).

hCHST15 siRNA entered into the draining lymph node after local injection, suppressed CHST15, and diminished MDSCs

To investigate whether locally injected hCHST15 siRNA possesses any effect on TDLN components directly or indirectly, we examined the pharmacokinetics of locally injected hCHST15 siRNA. Although locally injected CHST15 siRNA has been reported to be degraded

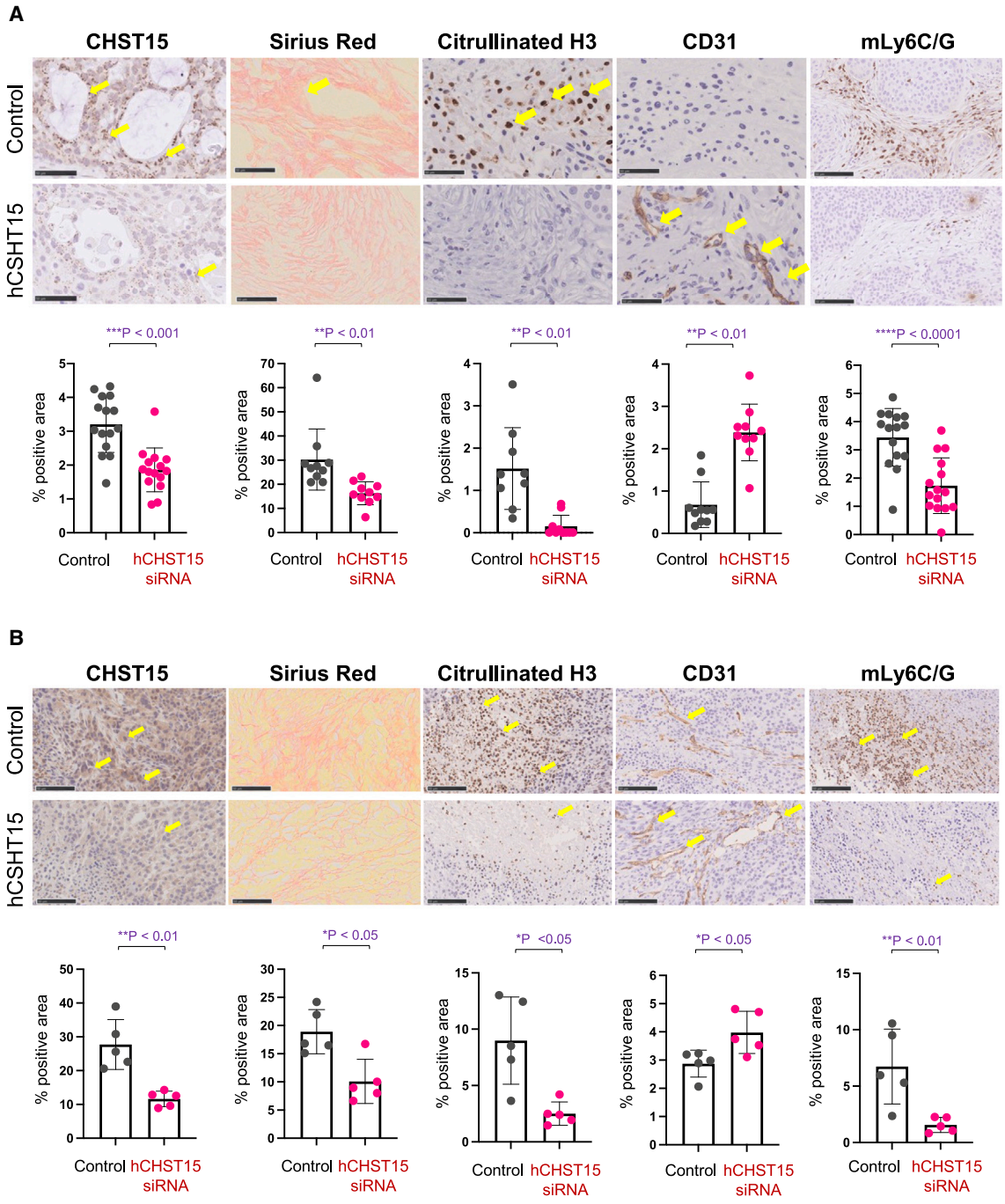

Figure 3. Silencing of hCHST15 siRNA alters stromal components in human BxPC-3 and mouse KPC models

(A and B, top) Immunostaining for CHST15, citrullinated histone H3 (Citrullinated H3), CD3 or mLy6C/G (brown) and Sirius red in the tumor of mice treated with vehicle control or hCHST15 siRNA. Scale bars, 20 μm. Yellow arrows indicate positive signals. (A and B) Quantitative analysis for stained tissues. Percentage positive areas for CHST15, Sirius red, citrullinated H3, CD31, and mLy6C/G are shown. Mean ± SD (n = 5). **p < 0.01, ***p < 0.001, ****p < 0.0001 by Wilcoxon rank-sum test.

rapidly after entering into the blood circulation,[30,34] hCHST15 siRNA was unexpectedly detected in not only the local sites, but also the draining lymph node after local injection (Figure 5A). In the KPC model, MDSCs were abundantly detectable in the TDLN, but this was significantly diminished by locally injected hCHST15 siRNA (Figures 5B and 5C). hCHST15 siRNA also suppressed CHST15 in

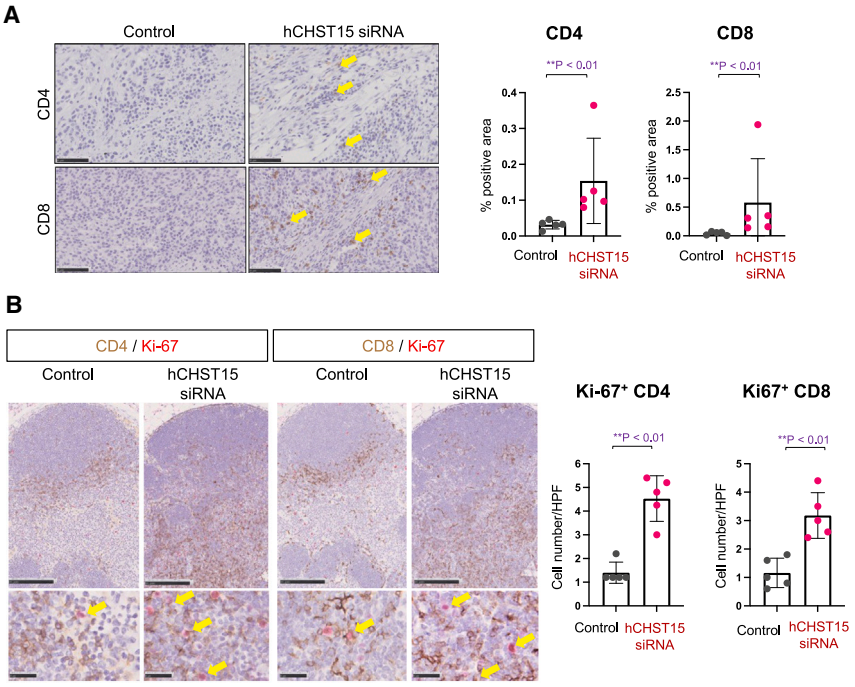

Figure 4. hCHST15 siRNA showed enhancement of T cells in both the tumor and TDLN in KPC model

(A) Immunostaining for CD4 or CD8 (brown) in the tumor of mice treated with vehicle control or hCHST15 siRNA in KPC model (left). Original magnification ×200. Yellow arrows indicate positive signals. Quantitative analysis for stained tissues (right). Percentage positive areas for CD4 and CD8 are shown. Mean ± SD (n = 5). **p < 0.01 by Mann-Whitney test. (B) Double immunostaining for Ki-67 (red) and CD4 (brown) or CD8 (brown) in the TDLN with vehicle control or hCHST15 siRNA in KPC model (left). Original magnification ×100 (top left), ×630 (bottom left). Yellow arrows indicate double-positive signals. Quantitative analysis for stained tissues (right). Percentage doubly positive areas for Ki-67$^+$CD4$^+$ and Ki-67$^+$CD8$^+$ are shown. Mean ± SD (n = 5). **p < 0.01 by Mann-Whitney test.

the TDLN (Figure 5B). Part of the MDSCs also expressed CHST15 in the TDLN, and this was reduced by locally injected hCHST15 siRNA (Figure S4A). In the BxPC-3 model, similar findings were observed, although the absolute numbers of MDSCs were low compared with the KPC model (Figure S4B).

Expression of CHST15 by human peripheral blood mononuclear cell-derived MDSC and direct action by hCHST15 siRNA

Finally, we investigated whether hCHST15 siRNA directly acts on MDSCs (Figure 6A). Human peripheral blood mononuclear cell (PBMC)-derived, IL-6, and granulocyte macrophage colony stimulating factor (GM-CSF)-induced CD33$^+$ MDSCs actually expressed CHST15 mRNA *in vitro* (Figure 6B). hCHST15 siRNA significantly suppressed CHST15 mRNA by CD33$^+$ MDSCs (Figure 6B). In addition, indoleamine 2,3-dioxygenase (IDO) mRNA was suppressed by hCHST15 siRNA (Figure 6B).

DISCUSSION

Intra-tumoral injection of STNM01 was shown to enhance TILs in chemotherapy-refractory patients with unresectable PDAC who showed a poor T cell immune suppressive condition.[25] In the present study, we investigated how intra-tumorally injected hCHST15 siRNA enhances TILs using xenogeneic and syngeneic mouse models of PDAC. We found that intra-tumorally injected hCHST15 siRNA acted not only locally, but also remotely. In a BxPC-3 xenograft model, depletion of local dense stroma alone was not effective in inducing tumor regression. In an immunocompetent KPC model, which showed tumor progression with poor TILs, hCHST15 siRNA achieved significant enhancement of TILs and this was associated with a significant increase in CD4$^+$ and CD8 T$^+$ cells in the TDLN compared with the control. Effective accumulation of TILs is thus considered to be achieved when an abundant number of T cells are generated in the secondary lymphoid organs, especially TDLN. This work is also the first report illustrating that CHST15 is expressed by tumor-associated MDSCs and the direct action of hCHST15 siRNA on MDSCs.

Locally, the major effects of hCHST15 siRNA are considered to be the suppression of CHST15 expression and the inhibition of tumor cell invasion, as observed in the present study. In addition, hCHST15 siRNA diminished Ly6C/G$^+$ MDSCs. In both BxPC-3 and KPC models, hCHST15 siRNA monotherapy by intra-tumoral injection inhibited stromal remodeling as evidenced by an altered fibrotic structure from dense to sparse, decreased NET formation, and increased vascularity. NET is recently reported to be a critical structure to interfere with CD8$^+$ cytotoxic T cell infiltration into cancer epithelium and is induced by PMN-MDSCs and neutrophils.[35] Decreased Ly6C/G$^+$ MDSCs by hCHST15 siRNA may thus lead to decreased NET formation. Hypovascularity is one of the unique features of PDAC, which leads to insufficient systemic drug delivery, blocks T cell entry, and is associated with a worse prognosis.[36] Although the molecular mechanisms remain unexplored, hCHST15 siRNA-mediated alteration of stromal structure may contribute to the maturation of vascularity, as fibrotic stroma is considered to inhibit the formation and function of blood vasculature.[37] Therefore, hCHST15 siRNA conditions the local tumor microenvironment to less NETosis with mature vascularity, which is a prerequisite for T cell entry.

Unexpectedly, we found that locally injected hCHST15 siRNA was detectable in the TDLNs. Remotely, a major effect of hCHST15 siRNA is considered to expand CD4$^+$ and CD8$^+$ T cells in the TDLN of the immunocompetent host. Direct action of hCHST15 siRNA on T cells is unlikely, since CHST15 was not expressed by LN T cells in the KPC model. In contrast, CHST15 was expressed by both human

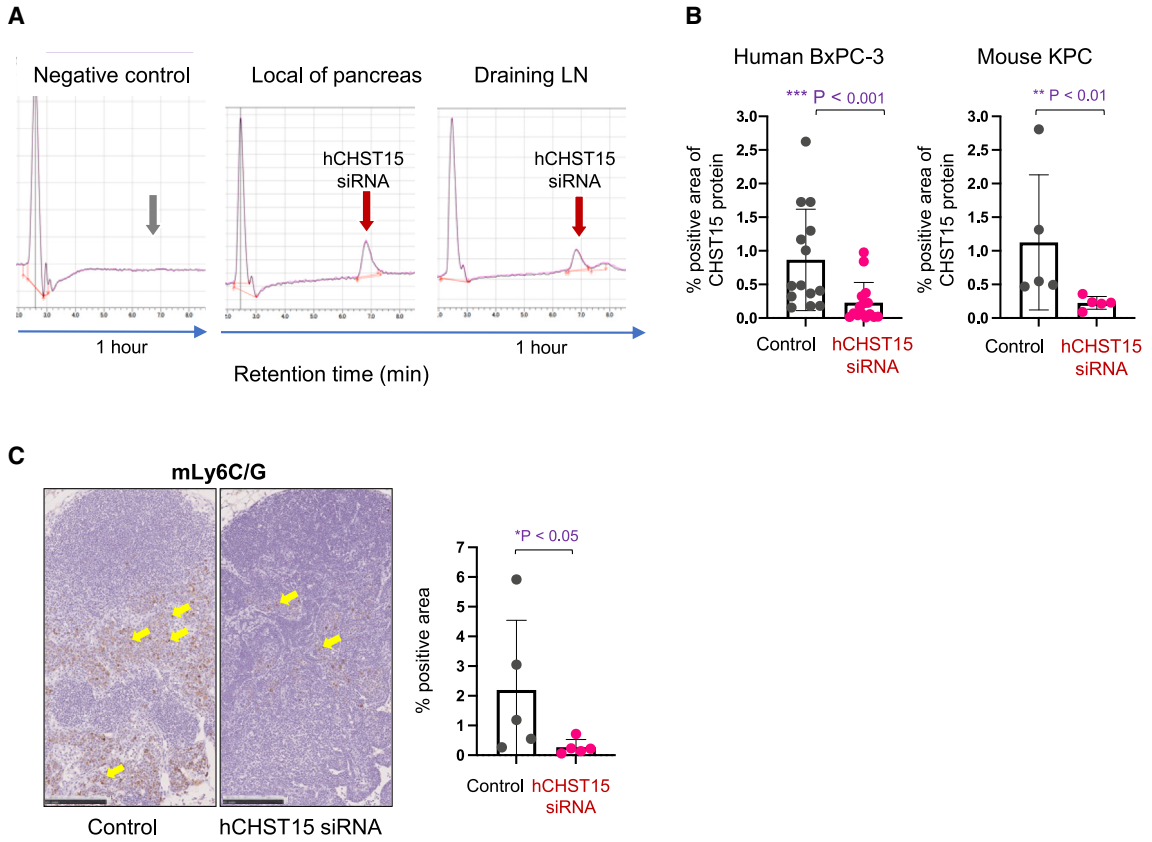

Figure 5. hCHST15 siRNA diminishes MDSCs in the TDLN

(A) Concentrations of hCHST15 siRNA within mouse tissues were detected by HLPC. Typical histograms of hCHST15 siRNA in the local tissue (pancreas) and its draining LN (paraaortic LN) 1 h after single local injection of hCHST15 siRNA are shown. Negative control shows HPLC result in the pancreas 1 h after single local injection of saline. (B) Quantitative analysis for CHST15-immunostained stained tissues of TDLN from human BxPC-3 model (left) or mouse KPC model (right). Percentage positive areas for CHST15 are shown. Mean ± SD (n = 15 for BxPC-3 model, n = 5 for KPC model). **p < 0.01, ***p < 0.001 by Mann Whitney test. (C) Immunostaining for Ly6C/G (brown) in the TDLN of KPC model (left panels). Original magnification ×100. Yellow arrows indicate positive signals. Quantitative analysis for stained tissues (right). Percentage positive areas for Ly6C/G are shown. Mean ± SD (n = 5). **p < 0.01 by Mann-Whitney test. LN, lymph node.

PBMC-derived and mouse MDSCs. hCHST15 siRNA acted on MDSCs and inhibited IDO expression *in vitro*. Direct action of hCHST15 siRNA on MDSCs in the TDLN is thus considered. Therefore, intra-tumorally injected hCHST15 siRNA enters into the TDLN through afferent lymphatics, diminishes MDSCs, removes MDSC-mediated T cell suppression, and expands $CD4^+$ and $CD8^+$ T cells in the TDLN. As it remains a challenge to convert an immune suppressive condition toward activation in PDAC, reactivation of T cells in secondary lymphoid organs would be a reasonable approach. The intra-tumoral route of administration is suggested to be an effective route for RNA oligonucleotide to reactivate T cells in the TDLNs.

We previously reported that TDLN-expanded T cells enter into the circulation, migrate to the tumor sites, and are further activated within the tumor sites, probably upon antigen encounter in the KPC implantation model.[26] Similarly, in the present study, hCHST15 siRNA-expanded T cells can accumulate in the tumor, contributing to T cell-dependent tumor growth inhibition. In PDAC patients, intra-tumoral administration of STNM01 was also reported to increase TILs.[25] The rate of RECIST-based progression disease (22.7%) was not so high considering reported clinical studies ranging from 46.8% to 91.6% for second-line setting,[38–43] and one complete response was observed.[25] This implies that locally acting STNM01 kept stable disease status for not only primary, but also metastatic, lesions and was able to eliminate metastatic tumors. Our results in the present study explain why local injection influences remote lesions. Since TDLN-expanded T cells enter the circulation, and then migrate to primary and metastatic lesions, it is also considered that these T cells play roles in preventing the progression or promoting the regression of tumors systemically.

There are some limitations in our study. First, the silencing efficacy of hCHST15 siRNA on mouse CHST15 mRNA was not strong (Figure 1B). This might influence the extent of anti-tumor efficacy in the mouse KPC model, although we found significant tumor growth inhibition by hCHST15 siRNA compared with controls (Figure 4B).

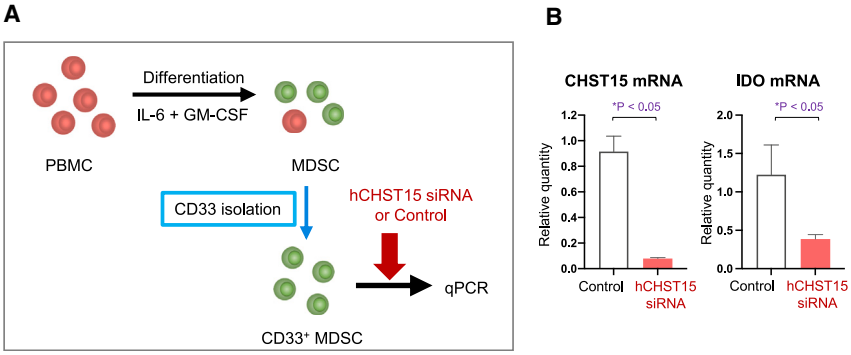

Figure 6. Expression of CHST15 by human PBMC-derived MDSC and direct action by hCHST15 siRNA

(A) *In vitro*, the efficacy of hCHST15 siRNA on the expression of human CHST15 mRNA and IDO mRNAs by human PBMC-derived CD33+ MDSCs are shown. (B) Relative quantity was measured compared with control by qPCR. *p < 0.05, Independent t test.

Second, although CHST15 was expressed by parts of MDSCs in both tumor and TDLN, hCHST15 siRNA broadly diminished MDSCs *in vivo*, including CHST15-negative MDSCs. It is possible that other mechanisms besides siRNA silencing of hCHST15 are responsible for this phenomenon. Since tumoral CHST15-derived CS-E is released into the circulation and leads to MDSC activation by binding to its functional receptor, CXCL4,[44,45] one possibility is considered that hCHST15 siRNA inhibits CS-E synthesis and indirectly diminishes MDSCs. Further investigations including MDSC mobilization will be required to explore the roles of hCHST15 siRNA on the modulation of tumor-emergent MDSCs. Third, our models did not show visible metastases, so the effect of hCHST15 siRNA on metastatic lesions needs to be investigated in other animal models. Forth, molecules related to immune checkpoint inhibition were not investigated. However, considering the findings that TILs increased in number by hCHST15 siRNA treatment, it will be of great interest to examine the detailed phenotype of T cells and the anti-tumor efficacy by combination with immune checkpoint inhibitors in mouse models. Fifth, the extent of MDSCs in the tumor-bearing control mice of C57BL/6 background was relatively higher than that of Balb/c background (Figure 3). Further investigations are needed into whether MDSCs with different strains[46,47] would modify the anti-tumor effect of hCHST15 siRNA.

In conclusion, *in vivo* coordinated actions of intra-tumorally injected hCHST15 siRNA to achieve effective TIL enhancement were documented in murine PDAC. Locally, hCHST15 siRNA suppresses stromal remodeling, which is a pivotal prerequisite for T cell entry, diffusion, recognition, and killing of cancer. At the same time, locally injected hCHST15 siRNA moves to the TDLN and remotely diminishes MDSCs while expanding T cells in the TDLN. A novel concept for an intra-tumoral route for RNA oligonucleotide is suggested to alter the suppressive microenvironment toward activation in addition to breaking dense stroma in this hard-to-treat PDAC.

MATERIALS AND METHODS

BxPC-3 xenograft model in T cell-deficient nude mice

A human PDAC cell line of BxPC-3 cells (ECACC 93120816) was used. Cells were grown in RPMI 1640 with 10% heat-inactivated fetal bovine serum, 100 U/mL penicillin, and 100 μg/mL streptomycin at 37°C under a humidified 5% CO_2 atmosphere.

BxPC-3 cells (1×10^7 cell/mouse) were implanted subcutaneously in T cell-deficient Balb/c-nu mice on day 0. CHST15 siRNA[26–32] (10 nmol/L; n = 15) or physiological saline as control vehicle (n = 15) was injected intra-tumorally (100 μL/mouse) twice a week from day 28 to day 42 and mice were sacrificed at day 42. The physiological saline was selected as a negative control to conduct experiments under the same conditions as a clinical trial.[34] Scrambled siRNA was not used, as we previously reported that there were no significant differences between scrambled siRNA and physiological saline in several murine models, including tumor implantation models to Balb/c-nu and C57BL/6J mice.[26,29–31] The dosing interval was determined by *in situ* hybridization and stem-loop PCR (Supporting materials and Figure S1). This study was approved by the Institutional Animal Care and Use Committee (Approval No. IACUC649-003) and was performed in accordance with the animal welfare bylaws of Shin Nippon Biomedical Laboratories, Ltd., which is accredited by AAALAC International.

KPC syngeneic model in immunocompetent mice

Mouse PDAC cell line of KPC cells (C57BL/6J background) were purchased from Ximbio (London, UK) and used as previously described.[26]

C57BL/6J mice (5-week-old males) were purchased from CLEA Japan, Inc. (Tokyo, Japan). KPC cells (5×10^4 cell/mouse) were subcutaneously injected into the left hind footpad of C57BL/6J mice. Tumor size was measured twice weekly using a caliper, and the tumor volume was determined using the formula, width2 × length × 0.5. CHST15 siRNA[27–32] (5.4 nmol/L, n = 5) or physiological saline as a control vehicle (n = 5) was intra-tumorally injected (100 μL/mouse) twice a week from day 7 to day 17, and mice were sacrificed at day 21. This study was approved by the Institutional Animal Care and Use Committee (Approval No. HKD49008) and was performed in accordance with the animal welfare by laws of HOKUDO, Co., Ltd. At the end of experiment, mice were euthanized and tumors and left popliteal lymph nodes (as TDLNs) were excised.

Immunohistochemistry

The tissues were fixed in 10% neutral buffered formalin, embedded in paraffin and were sliced serially into sections (3 μm thick) for hematoxylin and eosin, Sirius red, immunohistochemical staining, and immunofluorescence staining. Immunohistochemical staining was performed as previously reported[26,48,49] using CHST15, CD4, CD8α, mLy6C/G, CD31, CD11b, citrullinated histone H3, and

Ki-67. All antibodies used in the present study are listed in Table S1. For quantification of immunostained areas, bright field images were captured using a digital camera (DFC280, Leica Microsystems, Wetzlar, Germany) at 400-fold magnification and the positive areas or cell counts in five fields per section were measured using ImageJ software (National Institute of Health, Bethesda, MD, USA).[26,48,49]

In vitro silencing experiments of human PBMC-derived MDSCs, human PDAC, and murine PDAC cell lines

Human PBMC were purchased from Fujifilm Wako Pura Chemical Corporation (Richmond, VA, USA; Lot #2010113900) and were cultured in RPMI 1640 with 10% heat-inactivated fetal bovine serum, 100 U/mL penicillin, and 100 μg/mL streptomycin for 7 days, supplemented with recombinant human IL-6 (10 ng/mL, Fujifilm Wako Pura Chemical Corporation) and GM-CSF (10 ng/mL, Fujifilm Wako Pura Chemical Corporation) under humidified conditions in a CO_2 incubator set at 5% CO_2 conc1entration and 37°C.[50,51] After 1 week, all cells were collected from PBMC cultures. Adherent cells were removed using non-protease cell detachment solution Detachin (Genlantis, San Diego, CA, USA). $CD33^+$ cells were isolated from each culture using anti-CD33 magnetic microbeads and LS column separation (Miltenyi Biotec, Bergisch Gladbach, Germany) per the manufacturer's instructions.

The concentration of hCHST15 siRNA was 50 nM. We incubated 500 μL/well of Opti-MEMI (GIBCO, Waltham, MA, USA), siRNA, and 7.5 μL/well of RNAiMAX-Reagent (Invitrogen, Waltham, MA, USA) on a six-well plate at 25°C for 20 min. Isolated $CD33^+$ cells were suspended in 2.5 mL basic culture medium in a CO_2 incubator for 48 h (2.5 mL/well). Total RNA was extracted from each transfected cell using a FastPure RNA kit (Takara Bio Inc., Kusatsu, Japan) according to the manufacturer's instructions. The cDNA was synthesized and real-time RT-PCR was performed using SYBR premix Taq (Takara Bio Inc.). The expression of the human CHST15 gene or IDO was normalized by the expressed amount of RNA of human TATA Box Binding Protein. Human BxPC-3 cells and mouse KPC cells were treated in the same method and the expressions of human CHST15 genes and mouse CHST15 genes were measured as previously described.[26,30–34]

Melting temperature analysis

Binding affinities of the antisense strand of hCHST15 siRNA to human, pig, rat, and mouse mRNAs were analyzed by melting temperature using a UV/VIS absorption spectrophotometer UV-1650PC (Shimadzu, Kyoto, Japan) connected to a temperature controller. The thermal melting curve was prepared by measuring the absorbance of UV light at a wavelength of 260.0 nm in the temperature range of 20°C–100°C (measurement interval of 1°C, temperature increase rate of 1°C/min). A buffer solution containing 10 mM MOPS (pH 7.0) and 100 mM $NaNO_3$ was used in this experiment. Thermal melting curves of hybridized complexes between an antisense oligonucleotide (2 μL) and its target RNAs (2 μL) were measured. The melting temperatures (T_m) were determined by the least-squares method. The melting curves are calculated using the following equation.

$$A = (A_{t\,^\circ C} - A_{\min}) / (A_{\max} - A_{\min})$$

Detection of hCHST15 siRNA in mouse tissues

C57BL/6J mice (8 weeks old male) were purchased from CLEA Japan, Inc. We injected 30 μL 100 nM hCHST15 siRNA directly subcutaneously or into the pancreas tail of normal mice. One hour and 4 h later, mice were sacrificed (n = 2 per time point) and local tissues as well as draining lymph nodes were snap-frozen in liquid nitrogen for further analyses. The control group (n = 2 per time point) received PBS. Oligonucleotides were purified from frozen tissue samples using Clarity OTX methodology (Phenomenex, Inc., Torrance, CA, USA) according to the manufacturer's instructions.[52] The concentration of isolated oligonucleotides was then analyzed by HPLC using YMC-Triart C18 (YMC Co., Ltd., Kyoto, Japan).

Statistical analysis

Statistical analysis was performed using GraphPad PRISM version 9.0 software. For comparison variables, data was analyzed by Wilcoxon rank-sum test or Welch independent t test. A p value of less than 0.05 was considered to indicate statistical significance. Results were expressed as mean ± SD.

DATA AND CODE AVAILABILITY

The datasets used and/or analyzed during the current study available from the corresponding author on reasonable request.

SUPPLEMENTAL INFORMATION

Supplemental information can be found online at https://doi.org/10.1016/j.omton.2024.200812.

ACKNOWLEDGMENTS

We would like to acknowledge the significant contribution of our coauthor, Yoko Matsuda, who was the supervising author for this study. Prof. Matsuda, died on September 17, 2022.We also would like to express our sincere gratitude to Prof. Masayuki Nashimoto and Dr. Masayuki Takahashi (Research Institute for Healthy Living, Niigata University of Pharmacy and Applied Life Sciences, Niigata-shi, Niigata, Japan) for providing suggestions for stem-loop PCR methodology and design of primers. We thank Erina Momohara for her assistance in preparing the manuscript. This work was supported in part by a Grant-in-Aid for Scientific Research on Innovative Areas from the Japan Society for the Promotion of Science (JSPS) KAKENHI (Grant Number JP: 16H06277 to Y.M.; 19H03447, 23H02702 to F.S.) and Taiju Life Social Welfare Foundation to Y.M. and F.S.

AUTHOR CONTRIBUTIONS

Data curation: J.Y., F.S., H.Y, K.K., and Y.M.; funding acquisition: F.S., and K.K.; investigation: J.Y., F.S., K.Y., Y.M., M.K., and H.Y.; methodology: J.Y., F.S., K.Y., H.Y., J.K., M.K., N.Y., and Y.M.;

supervision: N.Y., F.S., and K.K.; writing – original draft, J.Y., H.Y., F.S., A.N., and K.K.; writing – review and editing: J.Y., H.Y., F.S., A.N., and K.K.

DECLARATION OF INTERESTS

H.Y. is the founder of TME Therapeutics Inc. M.K. received payments for lectures from Boston Scientific Japan, Olympus Japan, AstraZeneca, Takeda Pharmaceutical, EA Pharma, and Daiichi Sankyo, and supports for attending meetings from Olympus Japan. N.Y. received free provision of test agents from TME therapeutics, and a research grant for the present study from the Japan Agency for Medical Research and Development (AMED), research grants from Sanwa Kagaku Kenkyujo and Kaigen Pharma, and consulting fees from Olympus Japan, Top corporation, Fujifilm and Boston Scientific Japan, and payments for lectures from Olympus Japan, AstraZeneca, Daiichi Sankyo. Takeda Pharmaceuticals, Ohtsuka Pharmaceutical and EA Pharma.

REFERENCES

1. Ho, W.J., Jaffee, E.M., and Zheng, L. (2020). The tumour microenvironment in pancreatic cancer - clinical challenges and opportunities. Nat. Rev. Clin. Oncol. *17*, 527–540. https://doi.org/10.1038/s41571-020-0363-5.
2. Hosein, A.N., Brekken, R.A., and Maitra, A. (2020). Pancreatic cancer stroma: an update on therapeutic targeting strategies. Nat. Rev. Gastroenterol. Hepatol. *17*, 487–505. https://doi.org/10.1038/s41575-020-0300-1.
3. Halbrook, C.J., Lyssiotis, C.A., Pasca di Magliano, M., and Maitra, A. (2023). Pancreatic cancer: Advances and challenges. Cell *186*, 1729–1754. https://doi.org/10.1016/j.cell.2023.02.014.
4. Flies, D.B., Langermann, S., Jensen, C., Karsdal, M.A., and Willumsen, N. (2023). Regulation of tumor immunity and immunotherapy by the tumor collagen extracellular matrix. Front. Immunol. *14*, 1199513. https://doi.org/10.3389/fimmu.2023.1199513.
5. Xiao, Z., Todd, L., Huang, L., Noguera-Ortega, E., Lu, Z., Huang, L., Kopp, M., Li, Y., Pattada, N., Zhong, W., et al. (2023). Desmoplastic stroma restricts T cell extravasation and mediates immune exclusion and immunosuppression in solid tumors. Nat. Commun. *14*, 5110. https://doi.org/10.1038/s41467-023-40850-5.
6. Zhang, L., Conejo-Garcia, J.R., Katsaros, D., Gimotty, P.A., Massobrio, M., Regnani, G., Makrigiannakis, A., Gray, H., Schlienger, K., Liebman, M.N., et al. (2003). Intratumoral T cells, recurrence, and survival in epithelial ovarian cancer. N. Engl. J. Med. *348*, 203–213. https://doi.org/10.1056/NEJMoa020177.
7. Ino, Y., Yamazaki-Itoh, R., Shimada, K., Iwasaki, M., Kosuge, T., Kanai, Y., and Hiraoka, N. (2013). Immune cell infiltration as an indicator of the immune microenvironment of pancreatic cancer. Br. J. Cancer *108*, 914–923. https://doi.org/10.1038/bjc.2013.32.
8. Kiryu, S., Ito, Z., Suka, M., Bito, T., Kan, S., Uchiyama, K., Saruta, M., Hata, T., Takano, Y., Fujioka, S., et al. (2021). Prognostic value of immune factors in the tumor microenvironment of patients with pancreatic ductal adenocarcinoma. BMC Cancer *21*, 1197. https://doi.org/10.1186/s12885-021-08911-4.
9. Habuchi, O., Moroi, R., and Ohtake, S. (2002). Enzymatic synthesis of chondroitin sulfate E by N-acetylgalactosamine 4-sulfate 6-O-sulfotransferase purified from squid cartilage. Anal. Biochem. *310*, 129–136. https://doi.org/10.1016/s0003-2697(02)00277-4.
10. Mizumoto, S., Yamada, S., and Sugahara, K. (2015). Molecular interactions between chondroitin-dermatan sulfate and growth factors/receptors/matrix proteins. Curr. Opin. Struct. Biol. *34*, 35–42. https://doi.org/10.1016/j.sbi.2015.06.004.
11. ten Dam, G.B., van de Westerlo, E.M.A., Purushothaman, A., Stan, R.V., Bulten, J., Sweep, F.C.G.J., Massuger, L.F., Sugahara, K., and van Kuppevelt, T.H. (2007). Antibody GD3G7 selected against embryonic glycosaminoglycans defines chondroitin sulfate-E domains highly up-regulated in ovarian cancer and involved in vascular endothelial growth factor binding. Am. J. Pathol. *171*, 1324–1333. https://doi.org/10.2353/ajpath.2007.070111.
12. Vallen, M.J.E., Massuger, L.F.A.G., ten Dam, G.B., Bulten, J., and van Kuppevelt, T.H. (2012). Highly sulfated chondroitin sulfates, a novel class of prognostic biomarkers in ovarian cancer tissue. Gynecol. Oncol. *127*, 202–209. https://doi.org/10.1016/j.ygyno.2012.06.022.
13. Matsuda, Y., Fujii, Y., Matsukawa, M., Ishiwata, T., Nishimura, M., and Arai, T. (2019). Overexpression of carbohydrate sulfotransferase 15 in pancreatic cancer stroma is associated with worse prognosis. Oncol. Lett. *18*, 4100–4105. https://doi.org/10.3892/ol.2019.10764.
14. Ito, Z., Takakura, K., Suka, M., Kanai, T., Saito, R., Fujioka, S., Kajihara, M., Yanagisawa, H., Misawa, T., Akiba, T., et al. (2017). Prognostic impact of carbohydrate sulfotransferase 15 in patients with pancreatic ductal adenocarcinoma. Oncol. Lett. *13*, 4799–4805. https://doi.org/10.3892/ol.2017.6071.
15. Sugahara, K.N., Hirata, T., Tanaka, T., Ogino, S., Takeda, M., Terasawa, H., Shimada, I., Tamura, J.I., ten Dam, G.B., van Kuppevelt, T.H., and Miyasaka, M. (2008). Chondroitin sulfate E fragments enhance CD44 cleavage and CD44-dependent motility in tumor cells. Cancer Res. *68*, 7191–7199. https://doi.org/10.1158/0008-5472.Can-07-6198.
16. Kobayashi, T., Yan, H., Kurahashi, Y., Ito, Y., Maeda, H., Tada, T., Hongo, K., and Nakayama, J. (2013). Role of GalNAc4S-6ST in astrocytic tumor progression. PLoS One *8*, e54278. https://doi.org/10.1371/journal.pone.0054278.
17. Mizumoto, S., Takahashi, J., and Sugahara, K. (2012). Receptor for advanced glycation end products (RAGE) functions as receptor for specific sulfated glycosaminoglycans, and anti-RAGE antibody or sulfated glycosaminoglycans delivered in vivo inhibit pulmonary metastasis of tumor cells. J. Biol. Chem. *287*, 18985–18994. https://doi.org/10.1074/jbc.M111.313437.
18. Wang, X., Cheng, G., Zhang, T., Deng, L., Xu, K., Xu, X., Wang, W., Zhou, Z., Feng, Q., Chen, D., et al. (2020). CHST15 promotes the proliferation of TE-1 cells via multiple pathways in esophageal cancer. Oncol. Rep. *43*, 75–86. https://doi.org/10.3892/or.2019.7395.
19. Ito, Y., Watanabe, M., Nishizawa, T., Omachi, T., Kobayashi, T., Kasama, S., Habuchi, O., and Nakayama, J. (2007). The utility of formalin-fixed and paraffin-embedded tissue blocks for quantitative analysis of N-acetylgalactosamine 4-sulfate 6-O-sulfotransferase mRNA expressed by colorectal cancer cells. Acta Histochem. Cytoc. *40*, 53–59. https://doi.org/10.1267/ahc.07004.
20. Nadanaka, S., Kinouchi, H., and Kitagawa, H. (2018). Chondroitin sulfate-mediated N-cadherin/β-catenin signaling is associated with basal-like breast cancer cell invasion. J. Biol. Chem. *293*, 444–465. https://doi.org/10.1074/jbc.M117.814509.
21. Liu, L.C., Wang, Y.L., Lin, P.L., Zhang, X., Cheng, W.C., Liu, S.H., Chen, C.J., Hung, Y., Jan, C.I., Chang, L.C., et al. (2019). Long noncoding RNA HOTAIR promotes invasion of breast cancer cells through chondroitin sulfotransferase CHST15. Int. J. Cancer *145*, 2478–2487. https://doi.org/10.1002/ijc.32319.
22. Mizumoto, S., Watanabe, M., Yamada, S., and Sugahara, K. (2013). Expression of N-acetylgalactosamine 4-sulfate 6-O-sulfotransferase involved in chondroitin sulfate synthesis is responsible for pulmonary metastasis. BioMed Res. Int. *2013*, 656319. https://doi.org/10.1155/2013/656319.
23. Kawashima, H., Hirose, M., Hirose, J., Nagakubo, D., Plaas, A.H., and Miyasaka, M. (2000). Binding of a large chondroitin sulfate/dermatan sulfate proteoglycan, versican, to L-selectin, P-selectin, and CD44. J. Biol. Chem. *275*, 35448–35456. https://doi.org/10.1074/jbc.M003387200.
24. Cooney, C.A., Jousheghany, F., Yao-Borengasser, A., Phanavanh, B., Gomes, T., Kieber-Emmons, A.M., Siegel, E.R., Suva, L.J., Ferrone, S., Kieber-Emmons, T., and Monzavi-Karbassi, B. (2011). Chondroitin sulfates play a major role in breast cancer metastasis: a role for CSPG4 and CHST11 gene expression in forming surface P-selectin ligands in aggressive breast cancer cells. Breast Cancer Res. *13*, R58. https://doi.org/10.1186/bcr2895.
25. Fujisawa, T., Tsuchiya, T., Kato, M., Mizuide, M., Takakura, K., Nishimura, M., Kutsumi, H., Matsuda, Y., Arai, T., Ryozawa, S., et al. (2023). STNM01, the RNA oligonucleotide targeting carbohydrate sulfotransferase 15, as second-line therapy for chemotherapy-refractory patients with unresectable pancreatic cancer: An open label, phase I/IIa trial. EClinicalMedicine *55*, 101731. https://doi.org/10.1016/j.eclinm.2022.101731.

26. Ye, J., Suizu, F., Yamakawa, K., Mukai, Y., Kato, M., Yoneyama, H., Yahagi, N., and Matsuda, Y. (2023). Silencing of tumoral carbohydrate sulfotransferase 15 reactivates lymph node pancreatic cancer T cells in mice. Eur. J. Immunol. *53*, e2250160. https://doi.org/10.1002/eji.202250160.

27. Kiryu, H., Terai, G., Imamura, O., Yoneyama, H., Suzuki, K., and Asai, K. (2011). A detailed investigation of accessibilities around target sites of siRNAs and miRNAs. Bioinformatics *27*, 1788–1797. https://doi.org/10.1093/bioinformatics/btr276.

28. Nishimura, M., Matsukawa, M., Fujii, Y., Matsuda, Y., Arai, T., Ochiai, Y., Itoi, T., and Yahagi, N. (2018). Effects of EUS-guided intratumoral injection of oligonucleotide STNM01 on tumor growth, histology, and overall survival in patients with unresectable pancreatic cancer. Gastrointest. Endosc. *87*, 1126–1131. https://doi.org/10.1016/j.gie.2017.10.030.

29. Takakura, K., Shibazaki, Y., Yoneyama, H., Fujii, M., Hashiguchi, T., Ito, Z., Kajihara, M., Misawa, T., Homma, S., Ohkusa, T., and Koido, S. (2015). Inhibition of Cell Proliferation and Growth of Pancreatic Cancer by Silencing of Carbohydrate Sulfotransferase 15 In Vitro and in a Xenograft Model. PLoS One *10*, e0142981. https://doi.org/10.1371/journal.pone.0142981.

30. Suzuki, K., Arumugam, S., Yokoyama, J., Kawauchi, Y., Honda, Y., Sato, H., Aoyagi, Y., Terai, S., Okazaki, K., Suzuki, Y., et al. (2016). Pivotal Role of Carbohydrate Sulfotransferase 15 in Fibrosis and Mucosal Healing in Mouse Colitis. PLoS One *11*, e0158967. https://doi.org/10.1371/journal.pone.0158967.

31. Kai, Y., Tomoda, K., Yoneyama, H., Kitabatake, M., Nakamura, A., Ito, T., Yoshikawa, M., and Kimura, H. (2017). Silencing of Carbohydrate Sulfotransferase 15 Hinders Murine Pulmonary Fibrosis Development. Mol. Ther. Nucleic Acids *6*, 163–172. https://doi.org/10.1016/j.omtn.2016.12.008.

32. Watanabe, K., Arumugam, S., Sreedhar, R., Thandavarayan, R.A., Nakamura, T., Nakamura, M., Harima, M., Yoneyama, H., and Suzuki, K. (2015). Small interfering RNA therapy against carbohydrate sulfotransferase 15 inhibits cardiac remodeling in rats with dilated cardiomyopathy. Cell. Signal. *27*, 1517–1524. https://doi.org/10.1016/j.cellsig.2015.03.004.

33. Sato, H., Sagara, S., Nakajima, N., Akimoto, T., Suzuki, K., Yoneyama, H., Terai, S., and Yahagi, N. (2017). Prevention of esophageal stricture after endoscopic submucosal dissection using RNA-based silencing of carbohydrate sulfotransferase 15 in a porcine model. Endoscopy *49*, 491–497. https://doi.org/10.1055/s-0042-123189.

34. Suzuki, K., Yokoyama, J., Kawauchi, Y., Honda, Y., Sato, H., Aoyagi, Y., Terai, S., Okazaki, K., Suzuki, Y., Sameshima, Y., et al. (2017). Phase 1 Clinical Study of siRNA Targeting Carbohydrate Sulphotransferase 15 in Crohn's Disease Patients with Active Mucosal Lesions. J. Crohns Colitis *11*, 221–228. https://doi.org/10.1093/ecco-jcc/jjw143.

35. Zhang, Y., Chandra, V., Riquelme Sanchez, E., Dutta, P., Quesada, P.R., Rakoski, A., Zoltan, M., Arora, N., Baydogan, S., Horne, W., et al. (2020). Interleukin-17-induced neutrophil extracellular traps mediate resistance to checkpoint blockade in pancreatic cancer. J. Exp. Med. *217*, e20190354. https://doi.org/10.1084/jem.20190354.

36. Katsuta, E., Qi, Q., Peng, X., Hochwald, S.N., Yan, L., and Takabe, K. (2019). Pancreatic adenocarcinomas with mature blood vessels have better overall survival. Sci. Rep. *9*, 1310. https://doi.org/10.1038/s41598-018-37909-5.

37. Li, J., Wientjes, M.G., and Au, J.L.S. (2010). Pancreatic cancer: pathobiology, treatment options, and drug delivery. AAPS J. *12*, 223–232. https://doi.org/10.1208/s12248-010-9181-5.

38. Nagrial, A.M., Chin, V.T., Sjoquist, K.M., Pajic, M., Horvath, L.G., Biankin, A.V., and Yip, D. (2015). Second-line treatment in inoperable pancreatic adenocarcinoma: A systematic review and synthesis of all clinical trials. Crit. Rev. Oncol. Hematol. *96*, 483–497. https://doi.org/10.1016/j.critrevonc.2015.07.007.

39. Morizane, C., Okusaka, T., Furuse, J., Ishii, H., Ueno, H., Ikeda, M., Nakachi, K., Najima, M., Ogura, T., and Suzuki, E. (2009). A phase II study of S-1 in gemcitabine-refractory metastatic pancreatic cancer. Cancer Chemother. Pharmacol. *63*, 313–319. https://doi.org/10.1007/s00280-008-0741-7.

40. Wang-Gillam, A., Hubner, R.A., Siveke, J.T., Von Hoff, D.D., Belanger, B., de Jong, F.A., Mirakhur, B., and Chen, L.T. (2019). NAPOLI-1 phase 3 study of liposomal irinotecan in metastatic pancreatic cancer: Final overall survival analysis and characteristics of long-term survivors. Eur. J. Cancer *108*, 78–87. https://doi.org/10.1016/j.ejca.2018.12.007.

41. O'Reilly, E.M., Oh, D.Y., Dhani, N., Renouf, D.J., Lee, M.A., Sun, W., Fisher, G., Hezel, A., Chang, S.C., Vlahovic, G., et al. (2019). Durvalumab With or Without Tremelimumab for Patients With Metastatic Pancreatic Ductal Adenocarcinoma: A Phase 2 Randomized Clinical Trial. JAMA Oncol. *5*, 1431–1438. https://doi.org/10.1001/jamaoncol.2019.1588.

42. Marabelle, A., Le, D.T., Ascierto, P.A., Di Giacomo, A.M., De Jesus-Acosta, A., Delord, J.P., Geva, R., Gottfried, M., Penel, N., Hansen, A.R., et al. (2020). Efficacy of Pembrolizumab in Patients With Noncolorectal High Microsatellite Instability/Mismatch Repair-Deficient Cancer: Results From the Phase II KEYNOTE-158 Study. J. Clin. Oncol. *38*, 1–10. https://doi.org/10.1200/jco.19.02105.

43. Bockorny, B., Macarulla, T., Semenisty, V., Borazanci, E., Feliu, J., Ponz-Sarvise, M., Abad, D.G., Oberstein, P., Alistar, A., Muñoz, A., et al. (2021). Motixafortide and Pembrolizumab Combined to Nanoliposomal Irinotecan, Fluorouracil, and Folinic Acid in Metastatic Pancreatic Cancer: The COMBAT/KEYNOTE-202 Trial. Clin. Cancer Res. *27*, 5020–5027. https://doi.org/10.1158/1078-0432.Ccr-21-0929.

44. Petersen, F., Brandt, E., Lindahl, U., and Spillmann, D. (1999). Characterization of a neutrophil cell surface glycosaminoglycan that mediates binding of platelet factor 4. J. Biol. Chem. *274*, 12376–12382. https://doi.org/10.1074/jbc.274.18.12376.

45. Joseph, R., Soundararajan, R., Vasaikar, S., Yang, F., Allton, K.L., Tian, L., den Hollander, P., Isgandarova, S., Haemmerle, M., Mino, B., et al. (2021). CD8(+) T cells inhibit metastasis and CXCL4 regulates its function. Br. J. Cancer *125*, 176–189. https://doi.org/10.1038/s41416-021-01338-5.

46. Watanabe, H., Numata, K., Ito, T., Takagi, K., and Matsukawa, A. (2004). Innate immune response in Th1- and Th2-dominant mouse strains. Shock *22*, 460–466. https://doi.org/10.1097/01.shk.0000142249.08135.e9.

47. Youn, J.I., Nagaraj, S., Collazo, M., and Gabrilovich, D.I. (2008). Subsets of myeloid-derived suppressor cells in tumor-bearing mice. J. Immunol. *181*, 5791–5802. https://doi.org/10.4049/jimmunol.181.8.5791.

48. Yoneyama, H., Matsuno, K., Zhang, Y., Murai, M., Itakura, M., Ishikawa, S., Hasegawa, G., Naito, M., Asakura, H., and Matsushima, K. (2001). Regulation by chemokines of circulating dendritic cell precursors, and the formation of portal tract-associated lymphoid tissue, in a granulomatous liver disease. J. Exp. Med. *193*, 35–49. https://doi.org/10.1084/jem.193.1.35.

49. Kitazawa, Y., Ueta, H., Sawanobori, Y., Katakai, T., Yoneyama, H., Ueha, S., Matsushima, K., Tokuda, N., and Matsuno, K. (2019). Novel Targeting to XCR1(+) Dendritic Cells Using Allogeneic T Cells for Polytopical Antibody Responses in the Lymph Nodes. Front. Immunol. *10*, 1195. https://doi.org/10.3389/fimmu.2019.01195.

50. Lechner, M.G., Liebertz, D.J., and Epstein, A.L. (2010). Characterization of cytokine-induced myeloid-derived suppressor cells from normal human peripheral blood mononuclear cells. J. Immunol. *185*, 2273–2284. https://doi.org/10.4049/jimmunol.1000901.

51. Bronte, V., Brandau, S., Chen, S.H., Colombo, M.P., Frey, A.B., Greten, T.F., Mandruzzato, S., Murray, P.J., Ochoa, A., Ostrand-Rosenberg, S., et al. (2016). Recommendations for myeloid-derived suppressor cell nomenclature and characterization standards. Nat. Commun. *7*, 12150. https://doi.org/10.1038/ncomms12150.

52. Brown, K.M., Nair, J.K., Janas, M.M., Anglero-Rodriguez, Y.I., Dang, L.T.H., Peng, H., Theile, C.S., Castellanos-Rizaldos, E., Brown, C., Foster, D., et al. (2022). Expanding RNAi therapeutics to extrahepatic tissues with lipophilic conjugates. Nat. Biotechnol. *40*, 1500–1508. https://doi.org/10.1038/s41587-022-01334-x.

OMTON, Volume *32*

Supplemental information

Intra-tumoral administration of CHST15 siRNA remodels tumor microenvironment and augments tumor-infiltrating T cells in pancreatic cancer

Juanjuan Ye, Futoshi Suizu, Keiko Yamakawa, Yuri Mukai, Hiroyuki Yoneyama, Jiro Kondo, Motohiko Kato, Akira Nishiyama, Naohisa Yahagi, and Kyuichi Kadota

Supplemental Materials and Methods

In vitro silencing experiments

BxPC-3 cells (human PDAC cell line) were purchased form ECACC. The concentration of CHST15 siRNA was 50 nM. Five hundred μL/well of Opti-MEMl (GIBCO), siRNA and 7.5 μL/well of RNAiMAX-Reagent (Invitrogen) were incubated on a 6-well plate at 25°C for 20 minutes. BxPC-3 cells were suspended in 2.5 mL of the basic culture medium in a CO_2 incubator for 48 hours (2.5 mL/well). Total RNA was extracted from each transfected cell using a FastPure RNA kit (Takara Bio Inc.) according to the manufacturer's instructions. The cDNA was synthesized and real-time RT-PCR was performed using SYBR premix Taq (Takara Bio Inc.). The expression of the human CHST15 gene was normalized by the expressed amount of RNA of human GAPDH[1-3].

In vitro cell proliferation and invasion assay

Cell proliferation was measured by WST-1 assay as described previously[3]. Cell invasion was assessed using the CytoSelect 24-well Cell Invasion Assay (CELL BIOLABS, Inc., San Diego, CA). The lower chambers were filled with DMEM containing 10% FBS, and cells (2×10^4 cells/300 μL) in serum-free DMEM were placed in the upper chamber. After incubation for 24 h, invasive cells on the bottom of the invasion membrane were stained and quantified at OD 560nm in accordance with manufacture's instruction.

In vivo RISC-loading of and CHST15 mRNA cleavage by intratumorally injected CHST15 siRNA in BxPC-3 xenograft model

To determine the dosing interval of *in vivo* CHST15 siRNA, stem-loop PCR followed by RNA immunoprecipitation and *in situ* hybridization (ISH) were performed. Human PDAC cell line BxPC-3 cells (ECACC 93120816) were used. BxPC-3 cells ($1x10^7$ cell/mouse) were implanted subcutaneously to T cell-deficient Balb/c-nu mice on day 0. Single injection of CHST15 siRNA (10 nmol/L, n=6) or physiological saline as control vehicle (n=6) was performed intratumorally (100 μL/mouse) at day 12 and mice were sacrificed at days 14 (n=3/each) and 17 (n=3/each). This study was approved by the Institutional Animal Care and Use Committee (Approval No. IACUC649-009) and was performed in accordance with the animal welfare bylaws of Shin Nippon Biomedical Laboratories, Ltd., which is accredited by AAALAC International.

For stem-loop PCR followed by RNA immunoprecipitation, frozen tissues from day 17 [day 5 after dosing] were used. Ago2-binding RNA was purified from tumor tissue samples using MagCapture™ microRNA isolation kit, human Ago2 (FIJIFILM Wako Pure Chemical Corporation) according to the manufacture's instruction. Ago2-loaded siRNA was then quantified by stem-loop qPCR based on previously published methods[4, 5]. The following primers were used: antisense RT primer: GTCGTATCCAGTGCAGGGTCCGAGGTATTCGCACTGGATACGACATGGAG, sense RT primer: GTCGTATCCAGTGCAGGGTCCGAGGTATTCGCACTGGATACGACCTGATT, antisense forward primer: CGCGATTGTATTCATCTTGCTCTG, sense forward primer: CGCGGAGCAGAGCAAGATGAATAC, universal reverse primer: GTGCAGGGTCCGAGGTATTCG.

For ISH, formalin fixed paraffin embedded tissues samples from day 14 [day 2 after dosing] were used. BaseScope™ LS Red ISH assay (Advanced Cell Diagnostics, CA. USA) was performed by the manufacturer[6, 7]. For the detection of the CHST15 mRNA cleavage site by hCHST15 siRNA, short length probe was designed as follows: CAGCTCTGCAAAGGAGCAGAGCAAGATGAATACAATCATTATCGG. The cleavage site-containing mRNA was visualized as a dot led and the number of tumor cells positive for red signals in 5 filed/section at 400-fold magnification were measured using ImageJ software (National Institute of Health).

Table S1. List of primary antibodies used in the present study

Antibody [clone]	Source	Dilution
Rabbit anti-human CHST15 pAb	Merk	50
Rabbit anti-Citrullinated Histone H3 pAb	Abcam	5,000
Rabbit anti-mouse CD31 pAb	Abcam	100
Rat anti-mouse Ly6C/G mAb [RB6-8C5]	Arigo	50
Rabbit anti-mouse CD3 mAb [SP7]	Abcam	1,000
Rabbit anti-mouse CD8α mAb [EPR20305]	Abcam	1,000
Rabbit anti-mouse CD4 mAb [EPR19514]	Abcam	2,000

Table S2. Melting temperature of the hybridized complexes between an antisense oligonucleotide (ASO) and its target RNA sequences

Complex	Sequence *	MM	T_m (ºC)
Human/ASO	5'-GGAGCAGAGCAAGATGAAT-3' 3'-CCUCGUCUCGUUCUACUUA-5'	0	73
Pig/ASO	5'-GGA<u>A</u>CAGAGCAAGATGAAT-3' 3'-CCU<u>C</u>GUCUCGUUCUACUUA-5'	1	65
Rat/ASO	5'-G<u>C</u>AG<u>AC</u>GAGCAAGATGAAT-3' 3'-C<u>C</u>UC<u>GU</u>CUCGUUCUACUUA-5'	3	57
Mouse/ASO	5'-G<u>C</u>AGC<u>CC</u>AGCAAGATGAAT-3' 3'-C<u>C</u>UCG<u>UC</u>UCGUUCUACUUA-5'	3	54

* Mismatch (MM) bases are underlined.

A

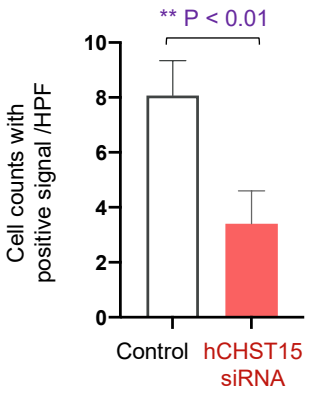

Day 2 post single dosing of vehicle control or hCHST15 siRNA.

B

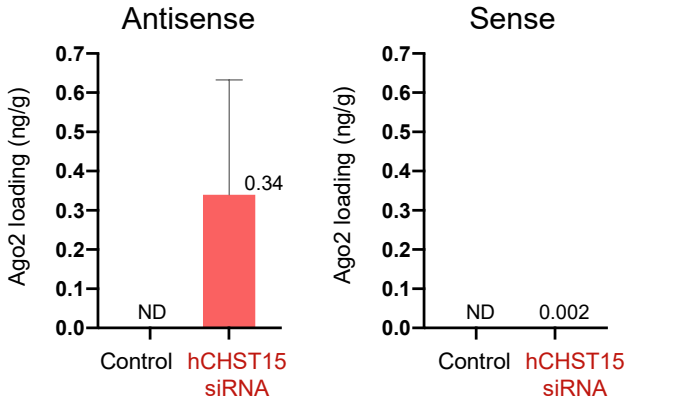

Average values (ng/g) are shown in the hCHST15 siRNA-treated mice (n=3) at Day 5 post single dosing.
N.D.: Not detected in the vehicle control-treated mice (n=3)

Figure S1. Cleavage of hCHST15 siRNA-binding site of CHST15 mRNA (A) and detection of RISC-loading sense and antisense strands of hCHST15 siRNA in tumor cells in vivo in human PDAC BxPC-3 cells.
A: Quantitative analysis of stained tissues by ISH. Short human mRNA sequence containing hCHST15 siRNA-cleavage site was stained by BaseCoreTM Red ISH assay. The number of cells with positive signals are shown. Mean ± SD (n=3). **p <0.01 by independent t test. **B:** RICS-loading sense or antisense strand of hCHST15 siRNA was measured by stem-loop PCR. Average values (ng/g) are shown in the control- or hCHST15 siRNA-treated mice (n=3). N.D.: Not detected in the Saline-treated mice (n=3).

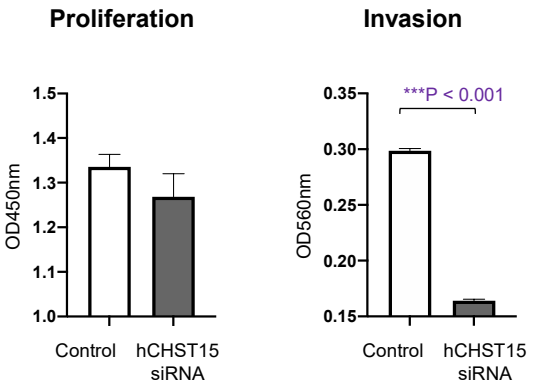

Figure S2. hCHST15 siRNA did not affect proliferation of BcPC-3 cells in vitro.
(Left) Proliferation of BxPC-3 cells treated with Saline as a control or 50 nM of hCHST15 siRNA. Mean ± SD (n=5). Not significant by Wilcoxon rank sum test. (right) Invasion of BxPC-3 cells treated with Saline as a control or 50 nM of CHST15 siRNA. Mean ± SD (n=2). ***p < 0.001 by Wilcoxon rank sum test.

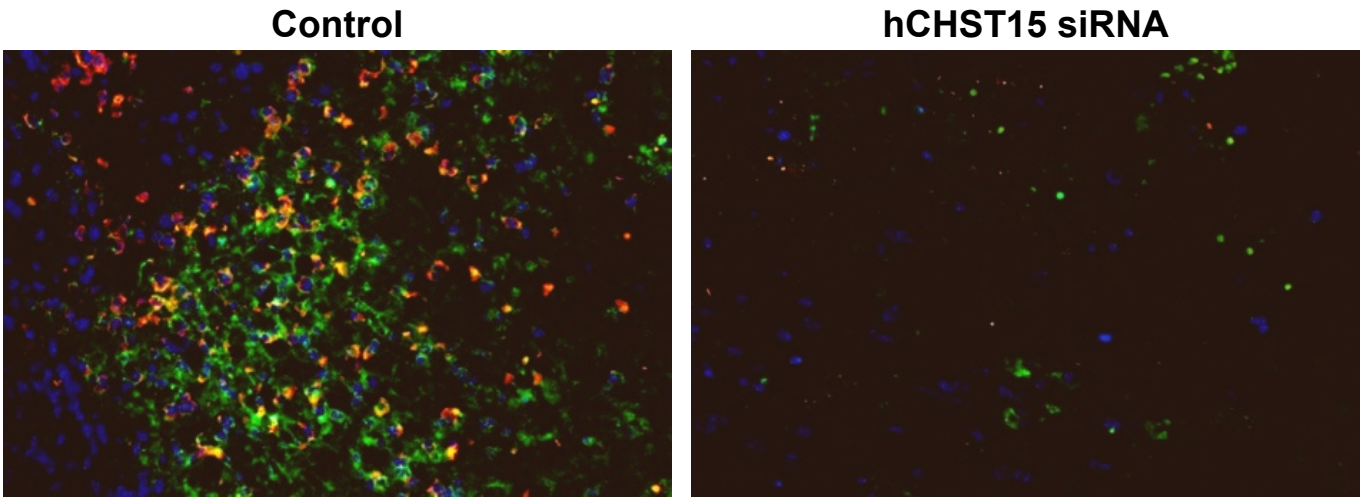

Figure S3. Part of tumoral MDSC expressed CHST15 and hCHST15 siRNA repressed MDSCs in the tumor. Immunostaining for CHST15 (red) and Ly6C/G (green) with DAPI (blue) in the tumor of KPC mice treated with control (left panel) or hCHST15 siRNA (right panel). Original magnification, x400.

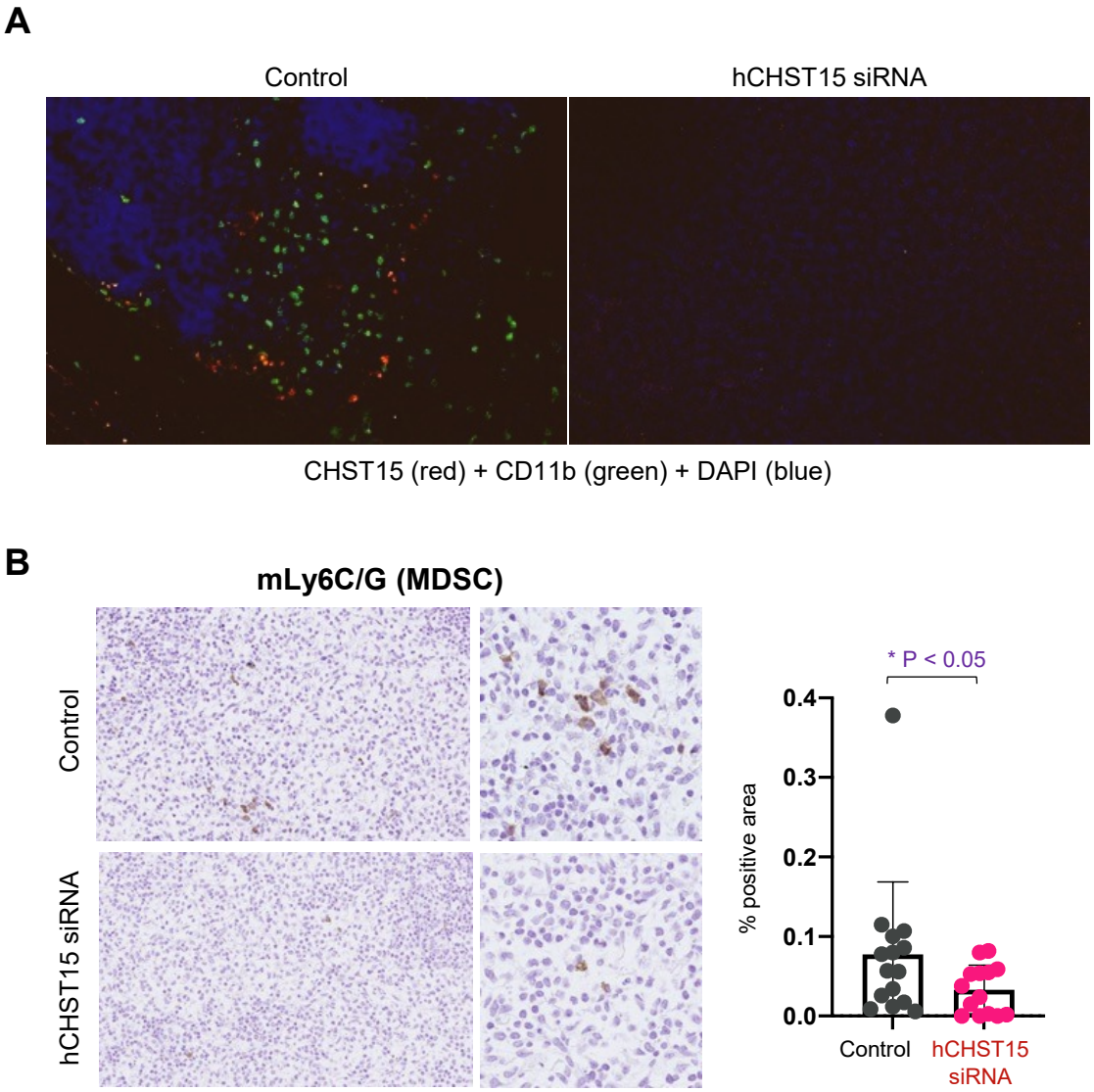

Figure S4. Part of TLDN MDSC expressed CHST15 and hCHST15 siRNA repressed MDSCs in the TDLN. **A.** Immunostaining for CHST15 (red) and CD11b (green) with DAPI (blue) in the TDLN of KPC mice treated with control (left panel) or hCHST15 siRNA (right panel). Original magnification, x200. **B:** Immunostaining for Ly6C/G (brown) in the TDLN of BxPC-3 mice treated with control (upper panel) or hCHST15 siRNA (lower panel). Original magnification, x200 (left), x630 (right). Quantitative analysis for stained tissues of control- (black dot) or hCHST15 siRNA (red bot)-treated mice. Percentage positive areas for Ly6C/G are shown. Mean ± SD (n=15). *p < 0.05 by independent t test.

References

1. Ye, J., Suizu, F., Yamakawa, K., Mukai, Y., Kato, M., Yoneyama, H., Yahagi, N., and Matsuda, Y. (2023). Silencing of tumoral carbohydrate sulfotransferase 15 reactivates lymph node pancreatic cancer T cells in mice. Eur J Immunol *53*, e2250160. 10.1002/eji.202250160.
2. Suzuki, K., Arumugam, S., Yokoyama, J., Kawauchi, Y., Honda, Y., Sato, H., Aoyagi, Y., Terai, S., Okazaki, K., Suzuki, Y., et al. (2016). Pivotal Role of Carbohydrate Sulfotransferase 15 in Fibrosis and Mucosal Healing in Mouse Colitis. PLoS One *11*, e0158967. 10.1371/journal.pone.0158967.
3. Takakura, K., Shibazaki, Y., Yoneyama, H., Fujii, M., Hashiguchi, T., Ito, Z., Kajihara, M., Misawa, T., Homma, S., Ohkusa, T., et al. (2015). Inhibition of Cell Proliferation and Growth of Pancreatic Cancer by Silencing of Carbohydrate Sulfotransferase 15 In Vitro and in a Xenograft Model. PLoS One *10*, e0142981. 10.1371/journal.pone.0142981.
4. Chen, C., Ridzon, D.A., Broomer, A.J., Zhou, Z., Lee, D.H., Nguyen, J.T., Barbisin, M., Xu, N.L., Mahuvakar, V.R., Andersen, M.R., et al. (2005). Real-time quantification of microRNAs by stem-loop RT-PCR. Nucleic Acids Res *33*, e179. 10.1093/nar/gni178.
5. Foster, D.J., Brown, C.R., Shaikh, S., Trapp, C., Schlegel, M.K., Qian, K., Sehgal, A., Rajeev, K.G., Jadhav, V., Manoharan, M., et al. (2018). Advanced siRNA Designs Further Improve In Vivo Performance of GalNAc-siRNA Conjugates. Mol Ther *26*, 708-717. 10.1016/j.ymthe.2017.12.021.

6. Guo, X., Zhao, Y., Nguyen, H., Liu, T., Wang, Z., and Lou, H. (2018). Quantitative Analysis of Alternative Pre-mRNA Splicing in Mouse Brain Sections Using RNA In Situ Hybridization Assay. J Vis Exp. 10.3791/57889.

7. Wu, S., Shi, X., Si, X., Liu, Y., Lu, T., Zhang, L., Liang, Z., and Zeng, X. (2019). EGFR T790M detection in formalin-fixed paraffin-embedded tissues of patients with lung cancer using RNA-based in situ hybridization: A preliminary feasibility study. Thorac Cancer *10*, 1936-1944. 10.1111/1759-7714.13169.